**Magnesium Technology 2011**
*Edited by: Wim H. Sillekens, Sean R. Agnew, Neale R. Neelameggham, and Suveen N. Mathaudhu*
***TMS (The Minerals, Metals & Materials Society), 2011***

# TWINNING MULTIPLICITY IN AN AM30 MAGNESIUM ALLOY UNDER UNIAXIAL COMPRESSION

Q. Ma[1], H. El Kadiri[1,2], A.L. Oppedal[1], J.C. Baird[1], M.F. Horstemeyer[1,2]
[1] Center for Advanced Vehicular Systems, Mississippi State University, Mississippi State, MS 39762, USA
[2] Department of Mechanical Engineering, Mississippi State University, Mississippi State, MS 39762, USA

Keywords: Texture; Magnesium; twinning; plasticity; EBSD

## Abstract

Twinning under compression along two perpendicular directions of an AM30 alloy with a $\{10\bar{1}0\}$ fiber texture was investigated. The primary extension $\{10\,\bar{1}\,2\}$ twinning occurred for both compression normal to the fiber and compression parallel to the fiber. These primary extension twins took forms of fully residual twins parallel to the fiber and the "stopped elastic" twins normal to the fiber. Both the $\{10\bar{1}1\}$-$\{10\bar{1}2\}$ and $\{10\bar{1}3\}$-$\{10\bar{1}2\}$ double twinning occurred in the matrix grains at the last stage of compression normal or parallel to the fiber, but as the "combined two shears" mode of the double twinning. Another time-sequence type of $\{10\bar{1}1\}$-$\{10\bar{1}2\}$ double twin also activated early normal to the fiber. The primary extension twinning and contraction twinning seem to obey the Schmid law according to the texture evolution.

## Introduction

Twinning is common in deformed magnesium due to insufficient independent slip systems necessary for arbitrary shape changes. The $\{10\,\bar{1}\,1\}$, $\{10\,\bar{1}\,2\}$, $\{10\,\bar{1}\,3\}$, $\{30\,\bar{3}\,4\}$ twins and so-called $\{10\bar{1}1\}$-$\{10\bar{1}2\}$ and $\{10\bar{1}3\}$-$\{10\bar{1}2\}$ double twins were reported in deformed magnesium single crystal or polycrystalline aggregates [1-5]. The $\{10\,\bar{1}\,2\}$ and $\{10\,\bar{1}\,1\}$ twins, known as extension twins and contraction twins, respectively, are by far the most common twins observed in nearly all magnesium alloys [1-5]. The twinning which occurred depended upon chemistry, texture and stress state of the material [6-9]. Although twins' presence and their effects on magnesium's mechanical behavior were reported in both experiments and simulations in literature [1,2,4,10], these results were usually concluded based on the final texture and/or microstructure and even on the habit plane trace analysis of twins [1-5]. The above literature indicates some uncertainty on twinning activation because the final texture and trace analysis of habit planes are not enough to reveal twinning activity in detail. As such, the intrinsic behavior of various twinning systems along strain increase under deformation requires further study, especially with said twinning systems undergoing different loading directions at various intermediate strains. We aim to study various twinning systems' behaviors from initiation of yield to rupture compression along two perpendicular directions of a magnesium alloy based on the macrotexture and microtexture of the alloy. Twinning sequence and twins' morphology are the study points in this article.

## Experimental Information

In this study, an extruded commercial magnesium AM30 billet (mass %, 2.54% Al, 0.40% Mn, Mg in balance) with a 178 mm diameter was selected as the experimental material. The simple uniaxial compression tests were conducted along the extrusion direction (ED) and the extrusion radial (defined as ERD) of the billet at strains -0.036, -0.06, -0.088 and rupture, respectively, at room temperature and strain rate $10^{-3}S^{-1}$. The third direction is defined as ETD. The ED and ERD cylindrical samples, with 6 mm in diameter and 6 mm in length, were cut by the electrical discharge machining (EDM) method from the AM30 billet along ED and ERD, respectively. For the results' consistency and stability, all the ED and ERD samples were cut in the same area which was near a mid-radius of the AM30 billet as shown in Figure 1a. The macrotexture and microtexture of the AM30 alloy at various strain levels were measured based on X-ray diffraction (XRD) and electron back-scattered diffraction (EBSD) techniques. Six pole figures $\{10\bar{1}0\}$, $\{0002\}$, $\{10\bar{1}1\}$, $\{10\bar{1}2\}$, $\{11\bar{2}0\}$ and $\{10\bar{1}3\}$ were characterized by a X-ray diffractometer Rigaku Smartlab using a reflection method, and background and defocusing effects were eliminated. The Orientation Distribution Functions (ODFs) were calculated based on the WIMV algorithm in the popLA package [11]. The complete pole figures and inverse pole figures were recalculated based on these ODFs and were plotted by the texture software MTEX [12]. The initial texture, based on XRD of the initial ED sample, is presented in Figure 1b. As shown in Figure 1b, this extruded AM30 alloy has a strong $\{10\bar{1}0\}$ fiber texture.

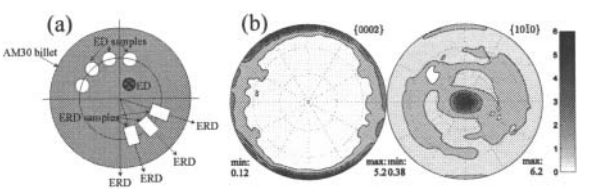


Figure 1: (a) The ED and ERD samples in the AM30 billet and (b) the initial texture of AM30 alloy based on XRD and the initial ED sample. The horizontal direction is the ETD and the ED is out of the paper.

## Results and Discussion

In the case of compression parallel to the $\{10\bar{1}0\}$ fiber, EBSD inverse pole figure (IPF) maps were used to investigate twinning development. Figure 2 shows the EBSD inverse pole figure (IPF) maps of ED samples at strains 0, -0.036, and -0.088. As shown in Figure 2, profuse $\{10\bar{1}2\}\langle 10\bar{1}0\rangle$ twinning activated within both the elongate parent grains and small equaxied recrystallized grains at strain -0.036. These zonal shape twins crossing the matrix grain boundaries from end to end are the typical residual twins [11]. Figure 2 also shows that almost all large grains have been totally twinned by the primary $\{10\bar{1}2\}$ twinning at strain -0.088. The inverse pole figures of ED based on XRD are presented in Figure 3 at various strain levels. We selected 200 grains to represent initial texture of AM30 (Figure 1b). As shown in Figure 2, the primary extension twinning $\{10\bar{1}2\}\langle 10\bar{1}0\rangle$ activated first in the matrix, and then the contraction twinning $\{10\bar{1}1\}\langle 10\bar{1}2\rangle$ and/or

the double twinning $\{10\bar{1}1\}$-$\{10\bar{1}2\}$ initiated in the twinned matrix grain in the rupture sample as shown in Figure 5. Accordingly, we assumed that the representative 200 grains evolved the $\{10\bar{1}2\}$ twinning first among 1: $(10\bar{1}2)[\bar{1}011]$, 2: $(1\bar{1}02)[\bar{1}101]$, 3: $(01\bar{1}2)[0\bar{1}11]$, 4: $(0\bar{1}12)[01\bar{1}1]$, 5: $(\bar{1}012)[10\bar{1}1]$, 6: $(\bar{1}102)[1\bar{1}01]$ according to the highest Schmid Factor (SF) of the twin variants. The second-order $\{10\bar{1}1\}$ twinning activated in the twinned grain as 1: $(10\bar{1}1)[10\bar{1}\bar{2}]$, 2: $(01\bar{1}1)[\ 01\bar{1}\bar{2}]$, 3: $(\bar{1}101)[\bar{1}10\bar{2}]$, 4: $(\bar{1}011)[\bar{1}01\bar{2}]$, 5: $(0\bar{1}11)[0\bar{1}1\bar{2}]$, 6: $(1\bar{1}01)[1\bar{1}0\bar{2}]$ with the highest SF value of the six $\{10\bar{1}1\}$ twin variants. The predicted primary $\{10\bar{1}2\}$ twins and second-order $\{10\bar{1}1\}$ twins are presented in Figure 3f. The $\{10\bar{1}2\}$ twinning and $\{10\bar{1}1\}$ twinning SFs under compression distribution in inverse pole figure are presented in Figure 4.

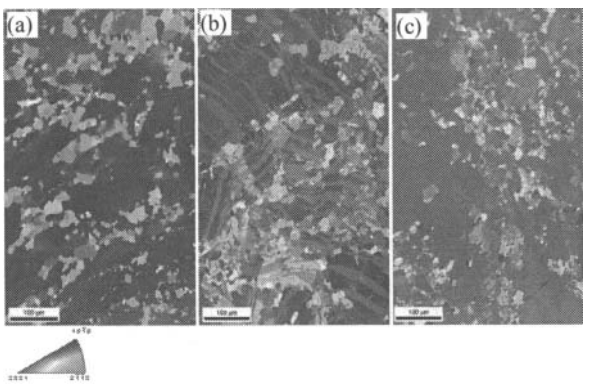


Figure 2: EBSD IPF maps of ED samples at strain (a) 0; (b) -0.036; (c) -0.088 showing $\{10\bar{1}2\}<10\bar{1}0>$ twin development. (The loading direction is out of paper. Inverse pole figure represents the ED direction.)

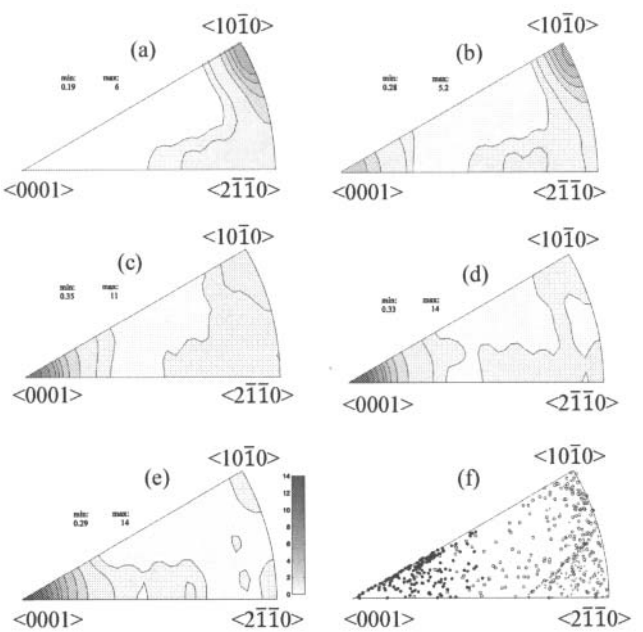


Figure 3: Inverse pole figures of AM30 alloy of ED at strain (a) 0; (b) -0.036; (c) -0.06; (d) -0.088; (e) rupture; (f) The primary $\{10\bar{1}2\}$ twins and the second-order $\{10\bar{1}1\}$ twins among the 200 representative grains compression along ED in inverse pole figure. The open circle symbols represent the initial 200 grains; the filled circle symbols represent the primary $\{10\bar{1}2\}$ twins; the cross symbols represent the secondary $\{10\bar{1}1\}$ twins.

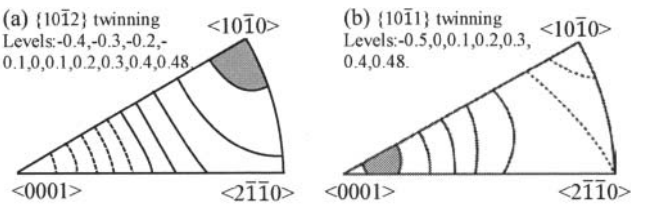


Figure 4: (a) The $\{10\bar{1}2\}$ twinning and (b) the $\{10\bar{1}1\}$ twinning Schmid Factor distribution under compression in inverse pole figure. (The shadow area notes SF >0.48; the dashed lines notes SF≤0.)

As shown in Figures 3a and 4a, the strong initial $<10\bar{1}0>$ fibre substantially favored the $\{10\bar{1}2\}$ twinning because it has a SF near the theoretical max value of 0.5. As a consequence, intensity around $<10\bar{1}0>$ quickly moved to <0001> area through primary $\{10\bar{1}2\}$ twinning (Figure 3f). As shown in Figure 4b, intensity around <0001> has also higher SF value for the $\{10\bar{1}1\}$ twinning; accordingly, the second-order $\{10\bar{1}1\}$ twinning would activate from strain about -0.088. Figures 3d and 3e illustrate that the third-order twinning could also initiated from strain -0.088, which was confirmed by the EBSD image quality map in Figure 5 below.

As for the $\{10\bar{1}1\}$ deformation twin, it is actually a degenerate compound twin with $K_1=\{10\bar{1}1\}$, $\eta_2=<30\bar{3}2>$, $K_2=\{10\bar{1}\bar{3}\}$, $\eta_1=<10\bar{1}\bar{2}>$ [13]. It has the plane of shear $\{1\bar{2}10\}$ that is a mirror plane, and the motif unit well lies in this plane of shear in this double lattice structure of magnesium. As such, simple shuffles of additional atoms movement all parallel to $\eta_1$ or normal to $K_1$ on shuffle mechanism and all atoms movement parallel to $\eta_1$ and $\eta_2$ on homogenous shear. As a consequence, the deformation $\{10\bar{1}1\}$ twinning with $K_1$, $\eta_1$, $K_2$, $\eta_2$ rational elements is favored by both a low twinning shear (0.137) and a simple shuffle mechanism even at a q=8 shuffle mode. However, the deformation $\{10\bar{1}1\}$ twins were observed rarely as single twins, but usually as double twins in matrix. Figure 5 shows some $\{10\bar{1}1\}$-$\{10\bar{1}2\}$ double twins and $\{10\bar{1}3\}$-$\{10\bar{1}2\}$ double twins in the ED rupture sample. However, these $\{10\bar{1}1\}$-$\{10\bar{1}2\}$ and $\{10\bar{1}3\}$-$\{10\bar{1}2\}$ double twins evolved in the matrix grains that have been totally twinned by the primary $\{10\bar{1}2\}$ twinning (Figure 2c). Specifically, third-order twinning occurred: $\{10\bar{1}2\}$-$\{10\bar{1}1\}$-$\{10\bar{1}2\}$ and $\{10\bar{1}2\}$-$\{10\bar{1}3\}$-$\{10\bar{1}2\}$ twinning activated in this case. The third-order twinning explains that the intensity around $<2\bar{1}\bar{1}0>$ in the inverse pole figure became weak in the rupture ED sample (Figure 3e).

In this study, the activated twinning system with $K_1=\{10\bar{1}3\}$, $K_2=\{10\bar{1}1\}$, $\eta_1=<30\bar{3}2>$, $\eta_2=<10\bar{1}2>$ is the reciprocal twinning of the $\{10\bar{1}1\}$ deformation twinning. The $\{10\bar{1}3\}$ twinning has the same plane of shear $\{1\bar{2}10\}$ and same twinning shear 0.137 with the $\{10\bar{1}1\}$ deformation twinning. Consequently, this $\{10\bar{1}3\}$ twinning was also favored due to the same reason mentioned above. However, the $\{10\bar{1}3\}$ deformation twinning is an extensional twinning [7,13] which could not activate in principle, in this case, under compression along *c*-axis of magnesium. The presence of $\{10\bar{1}3\}$-$\{10\bar{1}2\}$ twins in the ED rupture sample shown in Figure 5 implies a non-time-sequence activation of this double twinning. We found many $\{10\bar{1}3\}$-$\{10\bar{1}2\}$ and $\{10\bar{1}1\}$-$\{10\bar{1}2\}$ double twins in our other EBSD pictures of the ED rupture sample, existing together in the same twinned matrix grains similar to Figure 5.

This peculiar phenomenon is contradictory to the normal understanding of the double twinning mechanism that the secondary twin twins in the primary former twin. However, this special double twinning mechanism can be explained well by the Crocker's *Reciprocal Theorem* [14]. The Reciprocal theorem of double twinning mechanism of magnesium put forward by Crocker [14] in 1960s said: "If two double twinning mechanisms have first twinning shears which are either the same or reciprocal to each other and second twinning shears which are either the same or reciprocal to each other, then the resulting simple equivalent twinning modes are identical." According to the experimental observation (Figure 5) and Crocker's theory, the $\{10\bar{1}3\}$-$\{10\bar{1}2\}$ and $\{10\bar{1}1\}$-$\{10\bar{1}2\}$ double twins have the same simple double twinning mechanism: two shears plus one rotation in the plane of shear $\{1\bar{2}10\}$. In this case, the two shears must be combined together that means two shears evolving simultaneously because the primary $\{10\bar{1}3\}$ twin cannot exist independently under compression along *c*-axis of magnesium. As such, the $\{10\bar{1}3\}$-$\{10\bar{1}2\}$ and $\{10\bar{1}1\}$-$\{10\bar{1}2\}$ double twins should evolve in a process as: a small pre-existing or new nucleating $\{10\bar{1}3\}$ or $\{10\bar{1}1\}$ twin fault quickly retwins in the $\{10\bar{1}2\}$ twinning to the $\{10\bar{1}3\}$-$\{10\bar{1}2\}$ or $\{10\bar{1}1\}$-$\{10\bar{1}2\}$ double twin embryo, and this double twin embryo grows into the matrix grain. As such, we can call this double twinning mechanism as "combined two shears mechanism". This double twin system has a simple shear and an invariant plane strain similar with a simple normal twin system. The $\{10\bar{1}3\}$-$\{10\bar{1}2\}$ and $\{10\bar{1}1\}$-$\{10\bar{1}2\}$ double twin systems have the same shear of 0.258 with all four irrational twin elements [14]. The accommodation effect of this double twin system is not necessary in both the parent and the twin product [14], thus this mode is energetically favored. Accordingly, both $\{10\bar{1}3\}$-$\{10\bar{1}2\}$ and $\{10\bar{1}1\}$-$\{10\bar{1}2\}$ double twinning evolved as the combined two shears mode at the last stage under compression along ED, which may explain why single $\{10\bar{1}1\}$ or $\{10\bar{1}3\}$ primary twins were rarely observed in magnesium. In this study, the $\{10\bar{1}1\}$ or $\{10\bar{1}3\}$ twins in the tip of the double twins reported by Reed-Hill [1] were not observed in the ED rupture sample also validating this combined two shears mechanism. As shown in Figure 3, the activation of the primary $\{10\bar{1}2\}$ twinning seems to follow the Schmid law, but additional evidences are needed to validate the $\{10\bar{1}1\}$-$\{10\bar{1}2\}$ and $\{10\bar{1}3\}$-$\{10\bar{1}2\}$ twinning Schmid behavior.

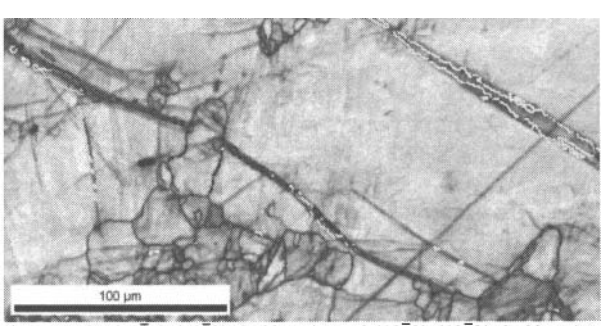


Figure 5: The $\{10\bar{1}1\}$-$\{10\bar{1}2\}$ double twins and $\{10\bar{1}3\}$-$\{10\bar{1}2\}$ double twins evolved in the same totally twinned matrix grain in the ED rupture sample. Fine black lines refer to grain boundaries >15°.

Axis angle pairs: 86±5°<11$\bar{2}$0>-----{10$\bar{1}$2}<10$\bar{1}$0>
38±5°<11$\bar{2}$0>-----{10$\bar{1}$1}-{10$\bar{1}$2}
22±5°<11$\bar{2}$0>-----{10$\bar{1}$3}-{10$\bar{1}$2}

With respect to compression normal to the $\{10\bar{1}0\}$ fiber, both inverse pole figures based on XRD and EBSD maps are used to investigate the twinning activation. Inverse pole figures of ERD at various strain levels based on XRD are presented in Figure 6. The primary $\{10\bar{1}1\}$ twins and the secondary $\{10\bar{1}2\}$ twins among the 200 representative grains under compression along ERD based on the highest SFs in inverse pole figure are presented in Figure 6f.

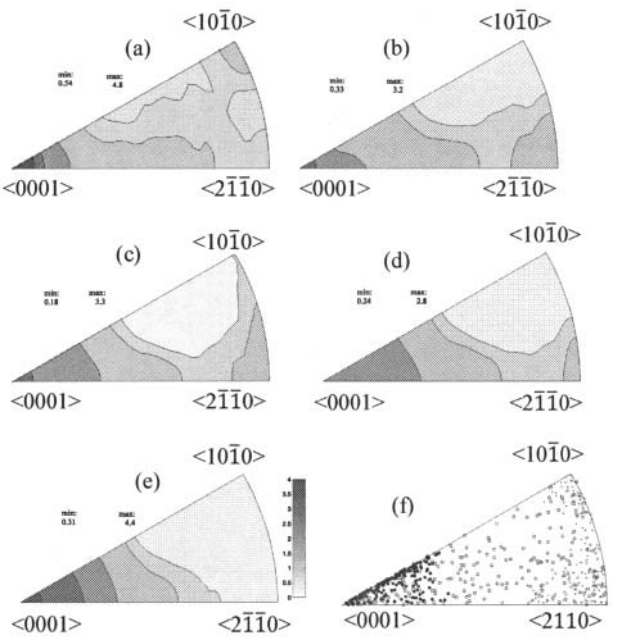


Figure 6: Inverse pole figures of AM30 alloy of ERD at strain (a) 0; (b) -0.036; (c) -0.06; (d) -0.088 and (e) rupture. (f) The primary $\{10\bar{1}1\}$ twins and the secondary $\{10\bar{1}2\}$ twins. The open circle symbols represent the initial 200 grains; the cross symbols represent the primary $\{10\bar{1}1\}$ twins; the filled circle symbols represent the secondary $\{10\bar{1}2\}$ twins.

As shown in Figure 6a and Figure 4, the primary $\{10\bar{1}2\}$ twinning and the primary $\{10\bar{1}1\}$ twinning will initiate simultaneously under compression along ERD. The intensity of <10$\bar{1}$0> weakened while <2$\bar{1}\bar{1}$0> intensity strengthened at same time along strain increase, as shown in Figure 6a, 6b and 6c. This measured result is consistent with Figure 6f, showing that the primary $\{10\bar{1}1\}$ twins will cause <2$\bar{1}\bar{1}$0> strength, while the primary $\{10\bar{1}2\}$ twins will result in <10$\bar{1}$0> weakness. Figures 6c, 6d and 6e show that the intensity of <2$\bar{1}\bar{1}$0> caused by primary $\{10\bar{1}1\}$ twinning annihilated again. Thus, the $\{10\bar{1}1\}$-$\{10\bar{1}2\}$ double twinning occurred starting from strain about -0.06 (Figure 6c), and a time-sequence of $\{10\bar{1}1\}$-$\{10\bar{1}2\}$ double twinning was clearly verified by <2$\bar{1}\bar{1}$0> intensity reduction from strain -0.06 to rupture. Moreover, this time-sequence of the $\{10\bar{1}1\}$-$\{10\bar{1}2\}$ twinning was confirmed further through EBSD analyses. As shown in Figure 7, a primary $\{10\bar{1}1\}$ twin was followed by a $\{10\bar{1}2\}$ twinning involved/contained within the $\{10\bar{1}1\}$ twin. Figure 7 substantially validated the sequence of the $\{10\bar{1}1\}$-$\{10\bar{1}2\}$ double twinning that the primary $\{10\bar{1}1\}$ contraction twinning activated first then the secondary extension $\{10\bar{1}2\}$ twinning evolved in the former contraction twin.

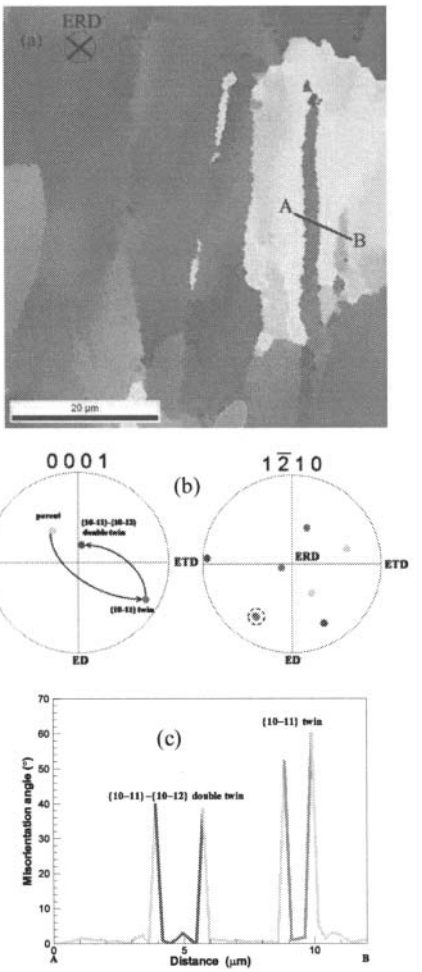


Figure 7: The primary $\{10\bar{1}1\}$ twin and the $\{10\bar{1}1\}$-$\{10\bar{1}2\}$ double twin in the ERD sample at strain -0.088 (a). The twinning sequence was proved by (b) the common rotation axis $<1\bar{2}10>$ and (c) the characteristic misorientation ~56° for $\{10\bar{1}1\}$ twinning and ~38° for $\{10\bar{1}1\}$-$\{10\bar{1}2\}$ twinning. The colors used here correspond to the colors of the IPF map in (a). The single $\{10\bar{1}1\}$ twin in (a) verified the time-sequence of $\{10\bar{1}1\}$-$\{10\bar{1}2\}$ double twinning in the ERD samples.

Some of the grains would evolve the primary $\{10\bar{1}2\}$ twinning and possibly the secondary $\{10\bar{1}1\}$ twinning according to the Schmid factor criteria in the case of compression along ERD. However, only the primary $\{10\bar{1}2\}$ twins were observed in the ERD sample, as shown in Figure 8a. The possible $\{10\bar{1}2\}$-$\{10\bar{1}1\}$ double twins cannot be found in ERD EBSD maps. The Schmid behavior suggests that the threshold stress of the $\{10\bar{1}1\}$ twinning evolved in the $\{10\bar{1}2\}$ twin should be very high, as it was in the ED sample at the last compression stage, but the stress compression along ERD cannot reach this required stress value. As a consequence, no $\{10\bar{1}2\}$-$\{10\bar{1}1\}$ double twinning occurred.

As shown in Figure 8a, the lenticular shape primary $\{10\bar{1}2\}$ twins exhibiting a tapering tip embedded within a matrix grain are the typical "stopped elastic" twins [13]. These stopped elastic twins did not disappear after stress removal due to the accommodation effect by slip systems in the matrix. The different forms of the extension $\{10\bar{1}2\}$ twins in the ED and ERD samples could result from the matrix grain morphology, necessary accommodation effect of twinning, neighbor grains shape and size and orientations.

Similar to the ED rupture sample, the $\{10\bar{1}3\}$-$\{10\bar{1}2\}$ and $\{10\bar{1}1\}$-$\{10\bar{1}2\}$ double twinning also occurred as the combined two shears mode at the last compression stage of ERD (Figure 8b). As shown in Figure 8b, the $\{10\bar{1}3\}$-$\{10\bar{1}2\}$ and $\{10\bar{1}1\}$-$\{10\bar{1}2\}$ double twins coexisted in the same matrix grain. Another important phenomenon, as shown in Figure 8b, is that the double twins preferentially favor the dynamic recrystallization (DRX) of magnesium, even at room temperature. In general, the active twinning systems in the ERD samples included the primary $\{10\bar{1}1\}$ twinning and the primary $\{10\bar{1}2\}$ twinning, the secondary $\{10\bar{1}2\}$ twinning and the last $\{10\bar{1}3\}$-$\{10\bar{1}2\}$ double twinning. The primary twinnings also seem to obey the Schmid factor criteria according to the texture evolution in Figure 6.

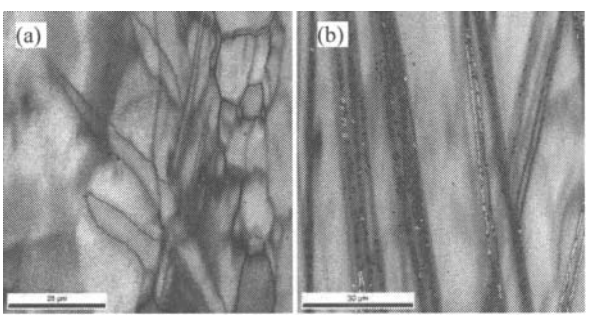


Figure 8: (a) The primary $\{10\bar{1}2\}$ twins in the ERD sample at strain -0.06 and (b) the $\{10\bar{1}1\}$-$\{10\bar{1}2\}$ and $\{10\bar{1}3\}$-$\{10\bar{1}2\}$ double twins in the ERD rupture sample. Fine black lines refer to grain boundaries >15°.
Axis angle pairs:
86±5°<11$\bar{2}$0>-----$\{10\bar{1}2\}$<$10\bar{1}0$>
38±5°<11$\bar{2}$0>-----$\{10\bar{1}1\}$-$\{10\bar{1}2\}$
22±5°<11$\bar{2}$0>-----$\{10\bar{1}3\}$-$\{10\bar{1}2\}$

## Conclusions

In summary, an extruded AM30 alloy exhibited twinning multiplicity under compression along two perpendicular directions. The active twinning systems compression parallel to the $\{10\bar{1}0\}$ fiber included the first primary $\{10\bar{1}2\}$ twinning, the $\{10\bar{1}1\}$-$\{10\bar{1}2\}$ and $\{10\bar{1}3\}$-$\{10\bar{1}2\}$ double twinning evolving as the combined two shears mechanism at the last compression stage. For compression normal to the $\{10\bar{1}0\}$ fiber, the primary $\{10\bar{1}2\}$ twinning and the primary $\{10\bar{1}1\}$ twinning first activated early, followed by the secondary $\{10\bar{1}2\}$ twinning evolving within the primary $\{10\bar{1}1\}$ twin. The combined two shears mode of $\{10\bar{1}3\}$-$\{10\bar{1}2\}$ and $\{10\bar{1}1\}$-$\{10\bar{1}2\}$ double twinning activated also at last stage. The extension $\{10\bar{1}2\}$ twin took the form of full residual twin compression parallel to the fiber and the form of "stopped elastic" twin normal to the fiber. All the primary twinning systems seem to obey the Schmid factor criteria.

## Acknowledges

The authors are grateful to the financial support from the Department of Energy, Contract No. DE-FC-26-06NT42755, and the Center for Advanced Vehicular Systems (CAVS) at Mississippi State University.

## References


1. R.E. Reed-Hill, "A study of the $\{10\bar{1}1\}$ and $\{10\bar{1}3\}$ twinning modes in magnesium," *Transactions of the Metallurgical Society of AIME,* 218 (1960), 554-558.
2. E.W. Kelley and W.F. Hosford Jr, "Plane-strain compression of magnesium and magnesium alloy crystals," *Transactions of the Metallurgical Society of AIME,* 242 (1968), 5-13.
3. B.C. Wonsiewicz and W.A. Backofen, "Plasticity of magnesium crystals," *Transactions of the Metallurgical Society of AIME,* 239 (1967), 1422-1431.
4. R.E. Reed-Hill and W.D. Robertson, "The crystallographic characteristics of facture in magnesium single crystals," *Acta Metallurgica,* 5 (1957), 728-737.
5. S.L. Couling, J.F. Pashak, and L. Sturkey, "Unique deformation and aging characteristic of certain magnesium-based alloys," *Transactions of the American Society of Metals,* 51 (1958), 94-104.
6. P.G. Partridge, "The crystallography and deformation modes of hexagonal close-packed metals," *Metallurgical Reviews,* 12 (1967), 169-194.
7. M.H. Yoo, "Slip, twinning, and fracture in hexagonal close-packed metals," *Metallurgical and Materials Transactions,* A12 (1981), 409-418.
8. M.R. Barnett, "Twinning and the ductility of magnesium alloys part I: "tension" twins," *Materials Science and Engineering,* A464 (2007), 1-7.
9. M.R. Barnett, "Twinning and the ductility of magnesium alloys part II: "contraction" twins," *Materials Science and Engineering,* A464 (2007), 8-16.
10. A. Jain and S.R. Agnew, "Modeling the temperature dependent effect of twinning on the behavior of magnesium alloy AZ31B sheet," *Materials Science and Engineering,* A462 (2007), 29-36.
11. J.S. Kallend et al., "Operational texture analysis," *Materials Science and Engineering,* A132 (1991), 1-11.
12. R. Hielscher and H. Schaeben, "A novel pole figure inversion method: specification of the MTEX algorithm," *Journal of Applied Crystallography,* 41 (2008), 1024-1037.
13. J.W. Christian and S. Mahajan, "Deformation twinning," *Progress in Material Science,* 39 (1995), 1-157.
14. A.G. Crocker, "Double twinning," *Philosophical Magazine,* 7 (1962), 1901-1924.